

Nearly defect-free dynamical models of disordered solids: The case of amorphous silicon

Raymond Atta-Fynn^{1, a)} and Parthapratim Biswas^{2, b)}

¹⁾Department of Physics, University of Texas at Arlington, Arlington, TX 76019

²⁾Department of Physics and Astronomy, The University of Southern Mississippi, Hattiesburg, MS 39406

It is widely accepted in the materials modeling community that defect-free realistic networks of amorphous silicon cannot be prepared by quenching from a molten state of silicon using classical or *ab initio* molecular-dynamics (MD) simulations. In this work, we address this long-standing problem by producing nearly defect-free ultra-large models of amorphous silicon, consisting of up to half-a-million atoms, using classical molecular-dynamics simulations. The structural, topological, electronic, and vibrational properties of the models are presented and compared with experimental data. A comparison of the models with those obtained from using the modified Wooten-Winer-Weaire bond-switching algorithm shows that the models are on par with the latter, which were generated via event-based total-energy relaxations of atomistic networks in the configuration space. The MD models produced in this work represent the highest quality of amorphous-silicon networks so far reported in the literature using molecular-dynamics simulations.

I. INTRODUCTION

Silicon continues to play a major role in the technological revolution of the 21st century. The recent developments of high-efficiency silicon-based heterojunction solar cells^{1,2} and two-qubit quantum logic gates in silicon,³ with applications to quantum computation, are indicative of its lasting importance for future technology. Unlike the crystalline state, the amorphous state of silicon is characterized by the presence of disorder in the radial and bond-angle distributions, along with a distinctly different topological (dis)ordering from its crystalline counterpart. Although a number of models based on the presence of small clusters of ordered materials – variously known as the paracrystalline model,^{4,5} the significant structure theory,⁶ and the crystalline hypothesis⁷ – have been proposed from time to time, a CRN model appears to be conceptually simple and representative of most of the characteristic properties of *a*-Si and *a*-Si:H, observed in experiments. It is now widely accepted that the structure of amorphous silicon can be described fairly accurately by the continuous-random-network (CRN) model of Zachariasen.⁸ The chemistry of silicon demands that an ideal CRN model of *a*-Si should satisfy the following properties: (i) every Si atom in the network must be bonded to four neighboring Si atoms; (ii) the network must exhibit a well-defined short-range order and possibly an intermediate-range order, the former being characterized by narrow bond-length and bond-angle distributions (e.g., the average bond angle and its variance should be close to 109.47° and 9°–11°, respectively); (iii) any deviation from the ideal 4-fold coordination of the atoms must be as minimal as possible, preferably 1–100 in 10⁵ atoms, so that the resulting electronic, optical, and vibrational properties, obtained from such a model of *a*-Si, are in agreement with experimental data. Following Weaire and Thorpe,⁹ and Heine,¹⁰ it can be shown, by employing a simple tight-binding Hamiltonian, that an atomistic model with these properties exhibits a gap

in the electronic spectrum. Despite these simple geometrical properties, atomistic modeling of defect-free *a*-Si networks, using molecular-dynamics simulations, has been proved to be particularly challenging and, at present, no defect-free large molecular-dynamics models of *a*-Si exist in the literature to our knowledge.

The current approaches to structural modeling of *a*-Si can be broadly classified into three categories. The first and foremost is based on Monte Carlo simulations, using the so-called bond-switching algorithm of Wooten, Winer and Weaire^{11,12} (W3). Here, one starts from a disordered silicon crystal with 100% 4-fold coordinated atoms and introduces a series of bond switches in the network, which are followed by total-energy relaxations using the Keating potential.¹³ The bond switching between a pair of atoms changes the network topology, but keeps the atomic-coordination number constant, by incorporating mostly 5- and 7-member rings in the network. A repeated application of bond switching, followed by total-energy relaxations, drives the system stochastically on the potential-energy surface (PES) from one local minimum to another over the energy barriers on the PES. In order for the system to be able to explore the relevant part of the configuration space, which is associated with topologically-distinct configurations than a crystal, it is necessary to conduct a minimal number of bond switches so that the system can escape from the initial (crystalline) state. An efficient implementation of the algorithm was presented by Barkema and Mousseau,¹⁴ where the method was modified to start from a random configuration and introducing local relaxations, upon bond switching, followed by intermittent total-energy relaxations of the network. The method is capable of generating large 100% defect-free *a*-Si networks with a very narrow bond-angle distribution.¹⁵

Molecular dynamics simulations, on the other hand, provide an alternative route, where one attempts to generate *a*-Si configurations by quenching from a molten state of Si at high temperature. Starting from a random configuration, with a mass density close to the experimental density¹⁶ of 2.25 g/cm³ for *a*-Si, the temperature of the system is increased well above the melting point at 1687 K of *c*-Si. After thermalization, the

^{a)}Electronic mail: attafynn@uta.edu

^{b)}Electronic mail: partha.biswas@usm.edu

temperature of the system is gradually reduced, typically at the rate of 5–10 K/ps, until the final temperature decreases to 300 K. The approach is commonly known as ‘quench-from-the-melt’ and it is particularly effective for amorphous solids having strong glass-forming ability. It has been observed that *a*-Si models obtained from the melt-quench approach contain a high density ($\geq 5\%$) of coordination defects, namely 3-fold and 5-fold coordinated atoms, which is at variance with the dangling-bond density (i.e., 3-fold coordinated atoms) estimated from electron spin resonance (ESR) measurements.¹⁷ Such a high density of coordination defects adversely affects the optoelectronic properties of the material, which renders MD models unsuitable for predictive studies of electronic and optical properties of *a*-Si and *a*-Si:H. The apparent failure of melt-quench approaches to produce satisfactory models of *a*-Si is not particularly surprising in view of the fact that *a*-Si is not a glass and that it is generally prepared in laboratories by vapor deposition on a cold substrate or by similar methods. The lack of *glassy* behavior in *a*-Si can be qualitatively understood from Phillips’ constraint-counting approach¹⁸ and Thorpe’s rigidity-percolation concept.¹⁹ In the latter, the glassy nature of a disordered solid was shown to be connected with the mean coordination number of the atoms in a network. Specifically, a disordered network with a mean coordination number $r_{av} < 2.4$ behaves as a *polymeric glass*, whereas networks with $r_{avg} > 2.4$, such as *a*-Si with $r_{avg} \approx 4$, behave like rigid *amorphous solids*. These observations, along with a high cooling rate and a rather short total simulation time, appear to indicate that realistic models of *a*-Si is unlikely to be produced by molecular-dynamics simulations. Thus, atomistic modeling of *a*-Si using direct MD simulations has attracted little attention in recent years²⁰ and a great majority of MD studies on *a*-Si were conducted in the past decades.^{21–29}

In the last decade, a number of hybrid approaches were developed that ushered in a new direction for modeling complex materials using information paradigm.^{30–34} These methods employ prior knowledge of materials from experiments, often in conjunction with structural,³⁵ chemical³⁶ and electronic³² constraints, and combine the information with an appropriate total-energy functional for structural determination of complex solids. Motivated by the Reverse Monte Carlo method^{37–41} and its drawback, where a three-dimensional structural model is generated by inverting one-dimensional experimental diffraction data, hybrid approaches go a step further by incorporating experimental data with a total-energy functional in search for structural solutions in an augmented solution space, so that the final structure is in agreement with both experiments and theory. Examples of such approaches include experimentally constrained molecular relaxation (ECMR),^{30,42} *ab initio* random structure searching (AIRSS),³⁴ first-principles assisted structural solutions (FPASS),³³ and force-enhanced atomic relaxations (FEAR).^{31,36} While the methods have achieved a remarkable success in determining structures of a variety of complex solids, none of the methods has been successful so far in producing high-quality, defect-free configurations of *a*-Si. In this paper, we have addressed this problem and pre-

sented a solution by producing nearly defect-free large models of amorphous silicon using molecular-dynamics simulations, supported by experimental evidence from X-ray diffraction and Raman spectroscopy.

The layout of the paper is as follows. In section II, we discuss a dynamical approach to modeling amorphous silicon using classical molecular-dynamics simulations in canonical and microcanonical ensembles, followed by *ab initio* total-energy relaxation within the framework of the density-functional theory. We successfully demonstrate that high-quality structural models of amorphous silicon, with defect concentrations as low as 0.7% and root-mean-square deviations (RMS) of bond angles below 10° , can be obtained directly from ultra-long MD simulations that last for several tens of nanoseconds. Section III discusses the results of our simulations with an emphasis on structural, electronic and vibrational properties of the models. We show that the results from the MD models are in excellent agreement with experimental data and that from the W3 models. This is followed by the conclusions of our work in section IV.

II. COMPUTATIONAL METHODOLOGY

A. Dynamical approach to *a*-Si using MD simulations

Classical molecular-dynamics simulations were performed for several systems ranging from 300 to 400,000 atoms. The details of the simulations are as follows. (i) *Initial random configurations*: Initial configurations of different sizes, $N = 300, 1000, 5000, 25000, 400,000$ Si atoms, were generated by randomly placing Si atoms in a cubic simulation box, subject to the constraint that the minimum separation between each pair of atoms was 2.1 Å. The length of the cubic simulation box was chosen such that the mass density matched with the experimental density¹⁶ of *a*-Si of 2.25 g/cm³. (ii) *MD simulations*: MD simulations, using the initial random configurations as input, were carried out in the canonical (NVT) and microcanonical (NVE) ensembles. The interatomic interaction between Si atoms were described using the modified Stillinger-Weber (SW) potential,^{43,44} which is given by,

$$V(R^N) = \frac{1}{2} \sum_{i=1}^N \sum_{\substack{j=1 \\ (j \neq i)}}^N v_2(r_{ij}) + \sum_{i=1}^N \sum_{\substack{j=1 \\ (j \neq i)}}^N \sum_{\substack{k=1 \\ (k \neq i) \\ (k > j)}}^N v_3(\mathbf{r}_{ij}, \mathbf{r}_{ik}), \quad (1)$$

where R^N indicates the atomic configuration and $v_2(r_{ij})$ is the two-body contribution to the potential energy given by,

$$v_2(r_{ij}) = \epsilon A \left[B \left(\frac{r_{ij}}{\sigma} \right)^{-p} - 1 \right] \exp \left(\frac{\sigma}{r_{ij} - a\sigma} \right) \times \Theta(a\sigma - r_{ij}), \quad (2)$$

TABLE I. Modified Stillinger-Weber potential energy parameters due to Vink *et al.*⁴³.

ϵ (eV)	λ	σ (Å)	γ	A	B	a	p
1.64833	31.5	2.0951	1.20	7.049556277	0.6022245584	1.80	4

and $v_3(\mathbf{r}_{ij}, \mathbf{r}_{ik})$ is the three-body contribution to the potential energy,

$$v_3(\mathbf{r}_{ij}, \mathbf{r}_{ik}) = \epsilon \lambda \exp \left(\frac{\sigma \gamma}{r_{ij} - a\sigma} + \frac{\sigma \gamma}{r_{ik} - a\sigma} \right) \times \left(\cos(\hat{\mathbf{r}}_{ij} \cdot \hat{\mathbf{r}}_{ik}) + \frac{1}{3} \right)^2 \times \Theta(a\sigma - r_{ij}) \Theta(a\sigma - r_{ik}), \quad (3)$$

with Θ being the Heaviside step function. Here, we have used the modified potential parameters, due to Vink *et al.*,⁴³ which are listed in Table I.

The equations of motion were integrated, using the velocity-Verlet algorithm, with a time step of $\Delta t = 1$ fs, and a chain of Nosé-Hoover thermostats^{45–47} was used to control the simulation temperature and the time evolution of the system in canonical ensembles. Each system was initially equilibrated at 1800 K for 50 ps and then it was cooled to 300 K, over a total time period of 600 ps, by gradually decreasing the temperature in steps of 100 K with an average cooling rate of 2.5 K per ps. At the end of the NVT-dynamics at 300 K, the system was subjected to evolve in a microcanonical ensemble (NVE) for an additional 50 ps so that the total simulation time for a single NVT-NVE cycle from an initial temperature of 1800 K to the final temperature of 300 K was 700 ps. The purpose of the NVE run was to eliminate any possible artifacts that could originate from the thermostats and to collect structural configurations during the NVE dynamics, which were free from any thermal fluctuations. Silicon configurations that satisfied a set of predefined criteria, such as those with a total potential energy and the density of coordination defects less than some prescribed values were collected during the 50-ps NVE run. On completion of the NVE run, the temperature of the system was increased to 1800 K to initiate the next NVT-NVE cycle. In order for the system to be able to explore a considerable part of the phase space in searching for better amorphous configurations, the NVT-NVE cycle was repeated many times until there were no significant changes in the total energy and density of coordination defects. In this study, we carried out 20–60 such cycles – depending on the size of the systems – for a duration of 700 ps per cycle, resulting in a total simulation time of 14–42 nanoseconds. To demonstrate the efficacy of such NVT-NVE cycles, we have plotted in Fig. 1 the time evolution of the potential energy per atom and the fraction of the 4-fold coordinated atoms at the end of each cycle versus the number of cooling cycles. For the purpose of demonstration only, the data shown in Fig. 1 were generated using a high value of the cooling rate, 5 K/ps, for a 1000-atom SW model. (iii) *Optimized configurations*: As mentioned before, a number of low-energy configurations with desired structural properties were collected during NVE evolution at the end of each

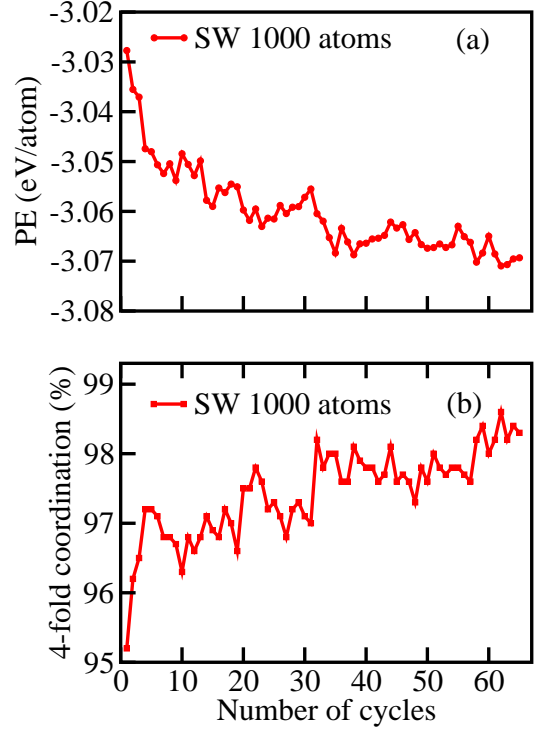


FIG. 1. (a) Time evolution of the potential energy per atom versus number of NVT-NVE cycles. In this illustrative plot, each cycle corresponds to a time period of 300 ps when the simulation temperature decreases from 1800 K to 300 K. (b) Evolution of the number of total atoms (in %) having 4-fold coordination versus the number of NVT-NVE cycles.

cycle in step (ii). The low-energy configurations were relaxed by minimizing the total energy using the modified SW potential with respect to the atomic positions. The energy minimization was carried out using the limited-memory BFGS algorithm.^{48,49} For comparison, W3 configurations¹¹ of sizes 300, 1000, and 5000 atoms, each with a mass density of 2.25 g/cm³, were also generated following the prescription of Barkema and Mousseau (see upper panel of Table II).

B. *Ab Initio* relaxation using density-functional theory

The electronic structure of the SW-optimized models of *a*-Si with 300, 1000, and 5000 atoms was studied using the local-basis density-functional code SIESTA.⁵⁰ Norm-conserving Troullier-Martins pseudopotentials,⁵¹ which were factorized in the Kleinman-Bylander form, were employed in this work.⁵² The 300- and 1000-atom models were optimized fully self-consistently using the Perdew-Burke-Ernzerhof (PBE)⁵³ formulation of the generalized-gradient approximation (GGA) of the exchange-correlation energy, and double- ζ with polarization (DZP) basis functions. For the model with 5000 atoms, we resorted to the Harris-functional approach,⁵⁴ which is based on the linearization of the Kohn-Sham equations in the density-functional theory. We also employed single- ζ (SZ) basis functions and the local density ap-

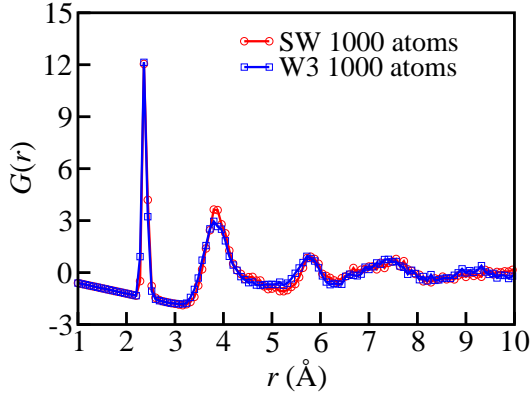


FIG. 2. (Color online) The variation of the reduced pair-correlation functions ($G(r)$) with radial distances (r) for 1000-atom SW (red) and W3 (blue) models.

proximation (LDA) to treat the exchange-correlation effects by using the Perdew-Zunger formulation of the LDA.⁵⁵ Similar SIESTA-based *ab initio* total-energy optimizations of W3 models of same sizes and mass density were also carried out for comparison with the SW models (cf. lower panel of Table II). The vibrational density of states of 1000-atom SW and W3 models was computed, using the harmonic approximation, by constructing the dynamical matrix of the system. The latter was obtained by computing the average atomic force on each atom via numerical differentiation of the total energy, using an atomic displacement of 5×10^{-3} Å. The resulting dynamical matrix was diagonalized to obtain the vibrational frequencies and eigenvectors.

III. RESULTS AND DISCUSSION

We begin by addressing the structural properties of the SW and W3 models. As mentioned earlier, the quality of CRN models of *a*-Si is primarily determined by: a) the radial distribution function; b) the bond-angle distribution (BAD) and its width; and c) the number of 4-fold coordinated atoms present in the network. A high-quality CRN model must satisfy all these properties simultaneously. The bond-angle distribution must have an width, $\Delta\theta$, in the range 9 – 11° and it must not have coordination defects more than 1 in 1000 atoms in order to be experimentally compliant. Currently, no MD models exist that can satisfy these requirements to our knowledge. In this section, we shall show that the MD models produced in our work, by combining NVT and NVE simulations discussed in Sec. IIA, closely satisfy all these requirements with a defect density of 0–1% and a root-mean-square (RMS) bond-angle width of 9 – 10° for models with size up to 1000 atoms. Figure 2 shows the reduced pair-correlation function (PCF), $G(r)$, versus radial distance (r) for SIESTA-optimized 1000-atom SW and W3 models of *a*-Si. The reduced PCF is defined as, $G(r) = 4\pi\rho r(g(r) - 1)$, where ρ is the number density of Si atoms and $g(r)$ is the conventional pair-correlation function. The reduced PCFs from the W3 and SW models matched closely in Fig. 2, showing an almost identical nature

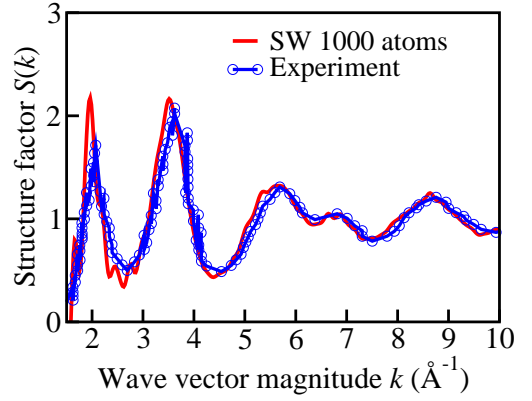


FIG. 3. (Color online) Comparison of the static structure factors of *a*-Si from molecular-dynamics simulations (SW) and high-energy X-ray diffraction. The experimental data (blue) correspond to annealed samples of *a*-Si from Laaziri *et al.*⁵⁶

of two-body correlations between the atoms in the respective models. This observation is also reflected in Fig. 3, where we have plotted the static structure factor,

$$S(k) = \left\langle \frac{1}{N} \sum_i \sum_j \exp[i\mathbf{k} \cdot (\mathbf{r}_i - \mathbf{r}_j)] \right\rangle, \quad (4)$$

of a 1000-atom SW model, along with the experimental structure-factor data for annealed samples of *a*-Si, due to Laaziri *et al.*⁵⁶ The symbol $\langle \rangle$ in Eq. 4 indicates the rotational averaging of the wave-vector transfer \mathbf{k} over a solid angle of 4π , along 20000 different directions. A slightly high value of the first-sharp-diffraction peak (FSDP) for the SW model could be attributed partly to the use of the classical SW potential, producing a pronounced structural ordering, and in part to instrumental broadening associated with the collection of X-ray diffraction data. A relatively slow cooling rate could also play a part in producing a somewhat more ordered structure. We shall return to this point later to discuss the topological order and ring statistics of the SW models.

Table II lists various structural properties of the SW and W3 models, from the average bond length and bond angle to the percentage of n -fold coordinated atom with $n = 3, 4$, and 5. We have used a cutoff value of 2.8 Å to calculate the coordination number of an atom, which corresponds to the first minimum of the PCF and it is practically identical for all models. The lower panel of Table II shows the results obtained from *ab initio* relaxations of the corresponding classical models. An examination of Table II shows that the SW models contain a small fraction of coordination defects. The percentage of 4-fold coordinated atoms can be seen to decrease only by 2% as the system size increase from 300 atoms to 400,000 atoms. The defect density in the 300- and 1000-atom models was found to be no more than 1% and, in each case, the RMS width ($\Delta\theta$) of the bond-angle distribution was observed to be less than 10° . To our knowledge, these are the best configurations so far obtained from any molecular-dynamics simulations to date. Although the models with 25000 and 400,000 Si atoms have a somewhat high defect concentration, in the

TABLE II. Structural properties of SW and W3 models. N , $\langle\theta\rangle$, $\Delta\theta$, $\langle n\rangle$, and C_k indicate the number of atoms, the average bond length (Å) and bond angle (degree), the RMS width of the bond angles (degree), the mean coordination number, and the percentage of k -fold coordinated atoms, respectively. SW and W3 denote the results from molecular-dynamics simulations and the bond-switching algorithm of Wooten, Winer and Weaire, respectively.^{11,12}

Model	N	d	$\langle\theta\rangle$	$\Delta\theta$	$\langle n\rangle$	C_3 (%)	C_4 (%)	C_5 (%)
W3 and SW-MD Models								
SW	300	2.38	109.22	9.06	4	0.3	99.3	0.3
W3	300	2.36	109.26	9.74	4	0	100	0
SW	1000	2.39	109.19	9.69	4	0.7	99	0.3
W3	1000	2.37	109.25	9.06	4	0	100	0.0
SW	5000	2.39	109.18	9.62	4	1.0	98	1.0
W3	5000	2.36	109.22	9.84	4	0	100	0
SW	25000	2.38	109.24	9.12	4	1.2	97.8	1.0
SW	400000	2.39	109.22	9.46	4	1.2	97.6	1.2
<i>Ab Initio</i> -relaxed W3 and SW-MD Models								
SW	300	2.38	109.20	9.44	4	0.3	99.3	0.3
W3	300	2.37	109.12	10.73	4	0	100	0
SW	1000	2.39	109.23	9.40	4	0.4	99	0.6
W3	1000	2.37	109.16	10.08	4	0	100	0.
SW	5000	2.39	109.19	9.49	4	1.0	98	1.0
W3	5000	2.37	109.11	10.71	4	0	100	0

range (2.2–2.4)%, the results can be readily appreciated in view of the large phase-space volume involved in the simulation of these ultra-large models. We should emphasize the fact that the MD models reported here were obtained from unconstrained atomic dynamics without using any coordination constraints unlike the W3 models, where a 4-fold nearest-neighbor list was always maintained during simulation.

Earlier we have mentioned that the PCF and the concentration of 4-fold coordinated atoms alone are not sufficient to determine the quality of CRN models of *a*-Si. For a high-quality CRN model, the distribution of bond angles must be sufficiently narrow, with an RMS width of the bond-angle distribution in the range 9–11°, as observed in X-ray⁵⁶ and Raman transverse-optic (TO) peak measurements.⁵⁷ Thus, in addition to the correct PCF, a CRN model of *a*-Si must have appropriate values of C_4 , $\langle\theta\rangle$, and $\Delta\theta$ so that the computed properties from the model are consistent with electron spin resonance,¹⁷ X-ray diffraction,⁵⁶ and Raman spectroscopy,⁵⁷ respectively. It is notable that all the reported values of $\Delta\theta$ for the SW models, including the one with 400,000 Si atoms, in Table II lie in the range of 9°–10°. The dihedral-angle distributions for the 1000-atom SW and W3 models are shown in Fig. 4. The distributions are quite similar with a characteristic peak at 60°.

Further characterization of SW and W3 models of *a*-Si is possible by examining the site-averaged orientational order parameter (OOP), Q_l , due to Steinhardt *et al.*⁵⁸ In spherical

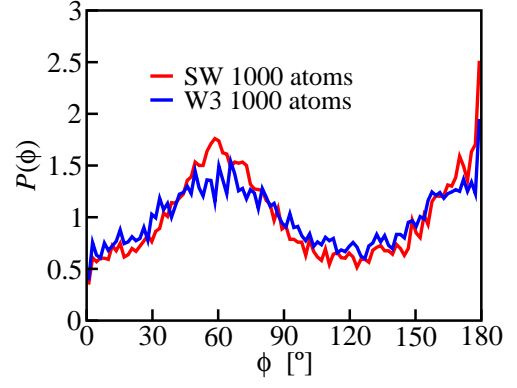


FIG. 4. (Color online) The distribution ($P(\phi)$) of dihedral angles (ϕ) in *a*-Si for SW (red) and W3 (blue) models of size 1000 atoms.

polar coordinates, the site-projected OOP is defined as,

$$Q_l^i = \sqrt{\frac{4\pi}{2l+1} \sum_{m=-l}^l \left| \frac{1}{n_i} \sum_{j \in \{n_i\}} Y_l^m(\theta(\mathbf{r}_{ij}), \phi(\mathbf{r}_{ij})) \right|^2}, \quad (5)$$

and the corresponding site-averaged value follows from,

$$Q_l = \frac{1}{N} \sum_{i=1}^N Q_l^i.$$

In Eq. (5), Q_l^i is the site-projected OOP associated with site i , whose value depends on the orientation of n_i bonds that extend from site i to the neighboring sites j . Here, N is the system size, and θ and ϕ are the polar and azimuthal angles of a bond \mathbf{r}_{ij} , respectively. Figure 5 show the magnitude of Q_l , $l = 1$ to $l = 8$, for SW, W3, and crystalline networks, each consisting of 1000 atoms. A crystalline silicon network (in diamond structure) is characterized by a null or zero value of Q_1 , Q_2 , and Q_5 . By contrast, SW and W3 models show a strong presence of Q_5 indicating the amorphous character of the networks. It is notable that Q_l values for SW and W3 models practically match with each other, reflecting an identical nature of local environment as far as the orientational ordering of the atoms in the first coordination shell (of an atom) is concerned.

Having addressed key structural properties of the SW models, we now examine their topological character in relation to the W3 models. Since the latter were generated by inducing, mostly, 5- and 7-member rings in a network, it is instructive to examine to what extent the ring statistics from W3 models, obtained from an event-based bond-switching algorithm, compare with the same from SW models. Toward that end, we have computed the number of n -member irreducible rings, from $n=3$ to $n=10$, and listed the values in Table III. Mathematically, an irreducible ring of size n is defined as the shortest, self-avoiding, irreversible path, which starts and ends at the same atomic site in n steps. Here, irreducibility refers to the fact that such a ring cannot be partitioned further into a smaller set of rings without changing the topology of the path

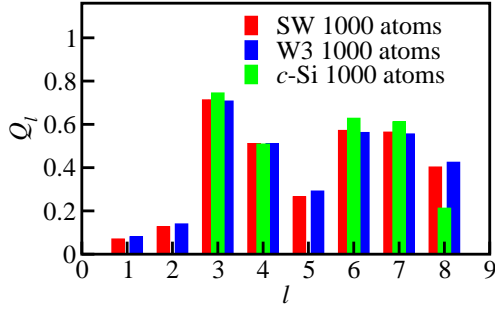


FIG. 5. (Color online) The site-averaged bond-orientational order parameter, Q_l , versus l for SW (red), W3 (blue), crystalline silicon (green) networks.

TABLE III. Irreducible ring statistics (rings/per atom) for SW and W3 models.

Model	N	4	5	6	7	8	9	10
W3 and SW-MD Models								
SW	1000	0.001	0.245	0.662	0.377	0.063	0.011	0.003
W3	1000	0.006	0.324	0.496	0.315	0.074	0.021	0.001
SW	5000	0.002	0.297	0.782	0.453	0.077	0.017	0.001
W3	5000	0.020	0.391	0.565	0.374	0.121	0.022	0.003
<i>Ab Initio</i> -relaxed W3 and SW-MD Models								
SW	1000	0.002	0.247	0.662	0.372	0.062	0.012	0.003
W3	1000	0.006	0.324	0.498	0.320	0.075	0.020	0.005
SW	5000	0.003	0.297	0.782	0.453	0.078	0.017	0.001
W3	5000	0.020	0.391	0.566	0.373	0.121	0.022	0.003

or circuit. Figure 6 presents a comparison of the ring-size distribution between an SW model and a W3 model of size 1000 atoms. In computing the irreducible ring-size distributions, we have not imposed periodic boundary conditions. Since crystalline silicon, without any defects, is characterized by 6-member rings only, the fraction of 6-member rings present in a network can be used as a measure of the degree of crystallinity of the network from a topological point of view. Thus, as far as the ring statistics of the W3 and SW models are concerned in Fig. 6, the latter can be described as having a somewhat pronounced topological ordering in comparison to the former. This observation is reflected in the FSDP of the SW models in Fig. 3.

A good atomistic configuration of *a*-Si must exhibit a gap in the electronic density of states (EDOS), irrespective of the method of preparation or modeling. The size of the gap depends on a number of factors, such as the density of coordination defects, the type of the defects (e.g., dangling and floating bonds), and the degree of disorder in the network. In general, a high density of 3-fold coordinated atoms or dangling bonds results in a large number of electronic states to appear near the Fermi level, which lead to a noisy or gap-less density of states. Figure 7 shows the EDOS for the 300- and 1000-atom SW and W3 models of *a*-Si, with the Fermi level at 0 eV. For the 300-atom SW model, we get a reasonably clean gap with two defects near the Fermi level, whereas the 1000-atom SW

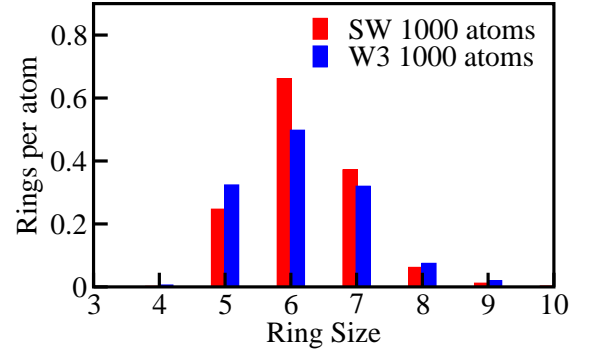


FIG. 6. (Color online) The distribution of irreducible rings/atom in SIESTA-relaxed 1000-atom SW (red) and W3 (blue) models. A high value of 6-member rings/atom in the SW model is indicative of a more topologically-ordered structure. See text for discussions.

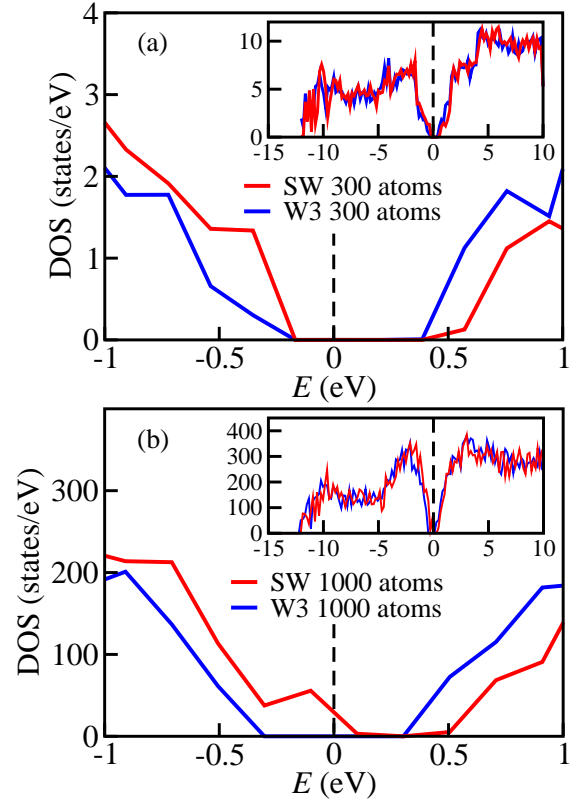


FIG. 7. (Color online) Depiction of the electronic densities of states (EDOS) of *a*-Si from SW (red) and W3 (blue) models in the regions close to their band-gaps. The full EDOS for the 300- and 1000-atom models are shown as inset in (a) and (b), respectively. The Fermi level is indicated by a dashed vertical line at 0 eV.

model produces a somewhat small gap due to 1% coordination defects. At any rate, a band gap of size 0.6-0.8 eV has been realized in the SW models. A few defects states that are present in the vicinity of the band-gap region can be readily passivated by hydrogenation to further improve the quality of the MD models.

Finally, a true atomistic model must reproduce correctly the

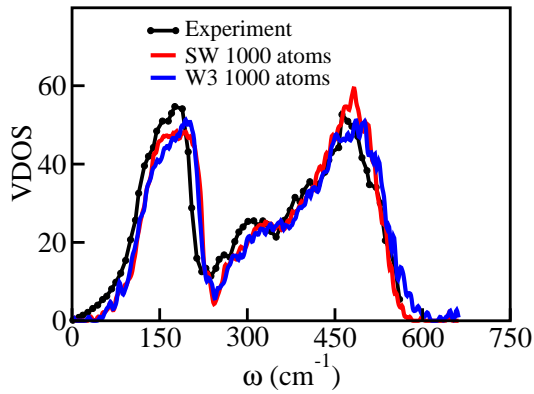


FIG. 8. (Color online) *Ab initio* vibrational densities of states from 1000-atom SW and W3 models. Inelastic neutron-scattering experimental data, due to Kamitakahara *et al.*,⁵⁹ are also included in the plot for comparison.

vibrational density of states (VDOS). Since vibrational excitations are more sensitive to local atomic environment than their electronic counterparts, any minute changes in the local atomic structure of *a*-Si can readily reflect on the VDOS at room temperature.⁶⁰ The VDOS was computed by constructing the force-constant (FC) matrix, using the harmonic approximation, and diagonalizing the corresponding dynamical matrix. Figure 8 shows the VDOS of *a*-Si, obtained from 1000-atom SW and W3 models. To compare the results with experimental data, we have also plotted the experimental inelastic neutron-scattering data from Kamitakahara *et al.*⁵⁹ The vibrational density of states from the SW and W3 models matches closely with the experimental data.

IV. CONCLUSIONS

In this paper, we have addressed a long-standing problem of structural modeling of *a*-Si using molecular-dynamics (MD) simulations. It is generally believed that, since *a*-Si is not a glass, direct MD simulations of *a*-Si, by quenching from a molten state of Si at high temperature, are not possible. A review of numerous MD studies on *a*-Si appears to support this conjecture by noting that MD simulations tend to produce a high density of coordination defects, which is inconsistent with the dangling-bond density observed in *a*-Si thin-films, by electron spin resonance measurements. This observation is consistent with the fact that *a*-Si samples are prepared in laboratories not by melt-quenching but by vapor deposition on a cold substrate or equivalent methods. Despite these observations, in this paper we have shown conclusively that it is possible to simulate high-quality CRN models of amorphous silicon by employing ultra-long molecular-dynamics simulations spanning several tens of nanoseconds. The size of the models produced in this study ranges from 300 atoms to 400,000 atoms and the corresponding defect density lies between 0.7% to 2.4%, respectively. All the MD models exhibit a very narrow bond-angle distribution, characterized by an average bond angle of $\sim 109.2^\circ$ and a root-mean-square (RMS) deviation

of $\sim 9.4^\circ$ – 9.7° . The latter is fully consistent with the value extracted from Raman TO peak measurements. Our results can be fully appreciated by noting that the 300-atom model has only a pair of defects – one dangling bond and one floating bond – and a bond-angle width of 9.44° , which exhibits a clean gap in the electronic density of states. On the other hand, the largest model with 400,000 atoms has a defect density of 2.4% only and an RMS width of 9.46° in the bond-angle distribution.

We conclude this section with the following observations. First, the availability of nearly defect-free MD models of *a*-Si brings considerable advantages in studying *a*-Si and *a*-Si-related materials. A molecular-dynamical approach provides a natural route to produce atomistic models of *a*-Si. The approach is simple and intuitive and it can be implemented easily and efficiently for large models, both in serial and parallel computing environments. Second, unlike the W3 method, a molecular-dynamical approach is free from any constraints. In the former, the system evolves from one configuration to another, by employing a limited set of bond switches, such that the coordination number of the atoms remains constant. While such bond reassignments can efficiently induce the requisite 5- and 7-member rings to produce the characteristic network topology of *a*-Si, the system can only explore a coarse-grained configuration space due to the coordination constraint and a limited combination of bond switches. Thus, the topological character of the resulting amorphous networks from such an approach may not be necessarily identical to the ones obtained from unconstrained MD simulations. This observation is reflected in the ring statistics obtained from the SW and W3 models. Since rings can play an important role in determining the stability and topological ordering of amorphous/disordered networks, it remains to be seen to what extent MD models and W3 models differ from each other and affect the material properties, involving higher-order correlation functions. Finally, the availability of large MD models will be particularly useful in studying silicon-heterojunction photovoltaic devices based on amorphous/crystalline interfaces.

ACKNOWLEDGMENTS

The work was supported by U.S. National Science Foundation under Grants No. DMR 1507166 and No. DMR 1507118. The authors thank Profs. Gerard Barkema (Utrecht, The Netherlands) and Normand Mousseau (Quebec, Canada) for providing their modified WWW code. The authors greatly appreciate the discussions with Profs. Stephen Elliott (Cambridge, UK) and David Drabold (Athens, Ohio). One of us (RAF) acknowledges the Texas Advanced Computing Center (TACC) at The University of Texas at Austin for providing HPC resources that have contributed to the results reported in this work.

¹M. Taguchi, A. Yano, S. Tohoda, K. Matsuyama, Y. Nakamura, T. Nishiwaki, K. Fujita, and E. Maruyama, *IEEE J. Photovolt.* **4**, 96 (2014).

²T. Mishima, M. Taguchi, H. Sakata, and E. Maruyama, *Sol. Energ. Mat. Sol. Cells* **95**, 18 (2011).

- ³M. Veldhorst, C. H. Yang, J. C. C. Hwang, W. Huang, J. P. Dehollain, J. T. Muhonen, S. Simmons, A. Laucht, F. E. Hudson, K. M. Itoh, A. Morello, and A. S. Dzurak, *Nature* **526**, 410 EP (2015).
- ⁴R. Hosemann and S. Bagchi, *Direct Analysis of Diffraction by Matter*, Series in Physics (North-Holland Pub. Co., 1962).
- ⁵The readers may note that paracrystalline models,⁶¹ i.e., CRN models containing small clusters of ordered Si atoms, were employed in the past to explain the origin of the intermediate-range order in *a*-Si, observed in Fluctuation Electron Microscopy.⁶² For an alternative explanation, based on voids in CRN models, see Refs. 63 and 64.
- ⁶J. Walter and H. Eyring, *The Journal of Chemical Physics* **9**, 393 (1941).
- ⁷G. Bartenev, *The structure and mechanical properties of inorganic glasses* (Wolters-Noordhoff, 1970).
- ⁸W. H. Zachariasen, *Journal of the American Chemical Society* **54**, 3841 (1932).
- ⁹D. Weaire and M. F. Thorpe, *Phys. Rev. B* **4**, 2508 (1971).
- ¹⁰V. Heine, *Journal of Physics C: Solid State Physics* **4**, L221 (1971).
- ¹¹F. Wooten, K. Winer, and D. Weaire, *Phys. Rev. Lett.* **54**, 1392 (1985).
- ¹²B. R. Djordjević, M. F. Thorpe, and F. Wooten, *Phys. Rev. B* **52**, 5685 (1995).
- ¹³P. N. Keating, *Phys. Rev.* **145**, 637 (1966).
- ¹⁴G. T. Barkema and N. Mousseau, *Phys. Rev. B* **62**, 4985 (2000).
- ¹⁵R. L. C. Vink, G. T. Barkema, M. A. Stijnman, and R. H. Bisseling, *Phys. Rev. B* **64**, 245214 (2001).
- ¹⁶J. S. Custer, M. O. Thompson, D. C. Jacobson, J. M. Poate, S. Roorda, W. C. Sinke, and F. Spaepen, *Applied Physics Letters* **64**, 437 (1994).
- ¹⁷M. H. Brodsky and R. S. Title, *Phys. Rev. Lett.* **23**, 581 (1969).
- ¹⁸J. Phillips, *Journal of Non-Crystalline Solids* **34**, 153 (1979).
- ¹⁹M. Thorpe, *Journal of Non-Crystalline Solids* **57**, 355 (1983).
- ²⁰A. Pedersen, L. Pizzagalli, and H. Jönsson, *New Journal of Physics* **19**, 063018 (2017).
- ²¹J. F. Justo, M. Z. Bazant, E. Kaxiras, V. V. Bulatov, and S. Yip, *Phys. Rev. B* **58**, 2539 (1998).
- ²²R. Car and M. Parrinello, *Phys. Rev. Lett.* **60**, 204 (1988).
- ²³D. A. Drabold, P. A. Fedders, O. F. Sankey, and J. D. Dow, *Phys. Rev. B* **42**, 5135 (1990).
- ²⁴N. Cooper, C. Goringe, and D. McKenzie, *Computational Materials Science* **17**, 1 (2000).
- ²⁵E. Kim and Y. H. Lee, *Phys. Rev. B* **49**, 1743 (1994).
- ²⁶I. Štich, R. Car, and M. Parrinello, *Phys. Rev. B* **44**, 11092 (1991).
- ²⁷P. Klein, H. M. Urbassek, and T. Frauenheim, *Computational Materials Science* **13**, 252 (1999).
- ²⁸M. D. Kluge, J. R. Ray, and A. Rahman, *Phys. Rev. B* **36**, 4234 (1987).
- ²⁹W. D. Luedtke and U. Landman, *Phys. Rev. B* **37**, 4656 (1988).
- ³⁰P. Biswas, R. Atta-Fynn, and D. A. Drabold, *Phys. Rev. B* **76**, 125210 (2007).
- ³¹A. Pandey, P. Biswas, and D. A. Drabold, *Scientific Reports* **6**, 33731 EP (2016).
- ³²K. Prasai, P. Biswas, and D. A. Drabold, *Scientific Reports* **5**, 15522 EP (2015).
- ³³B. Meredig and C. Wolverton, *Nature Materials* **12**, 123 EP (2012).
- ³⁴C. J. Pickard and R. J. Needs, *Journal of Physics: Condensed Matter* **23**, 053201 (2011).
- ³⁵P. Biswas and S. R. Elliott, *Journal of Physics: Condensed Matter* **27**, 435201 (2015).
- ³⁶A. Pandey, P. Biswas, and D. A. Drabold, *Phys. Rev. B* **92**, 155205 (2015).
- ³⁷R. L. McGreevy and L. Pusztai, *Molecular Simulation* **1**, 359 (1988).
- ³⁸O. Gereben and L. Pusztai, *Phys. Rev. B* **50**, 14136 (1994).
- ³⁹J. K. Walters and R. J. Newport, *Phys. Rev. B* **53**, 2405 (1996).
- ⁴⁰P. Biswas, R. Atta-Fynn, and D. A. Drabold, *Phys. Rev. B* **69**, 195207 (2004).
- ⁴¹M. J. Cliffe, A. P. Bartók, R. N. Kerber, C. P. Grey, G. Csányi, and A. L. Goodwin, *Phys. Rev. B* **95**, 224108 (2017).
- ⁴²P. Biswas, D. N. Tafen, and D. A. Drabold, *Phys. Rev. B* **71**, 054204 (2005).
- ⁴³R. L. C. Vink, G. T. Barkema, W. F. van der Weg, and N. Mousseau, *Journal of Non-Crystalline Solids* **282**, 248 (2001).
- ⁴⁴F. H. Stillinger and T. A. Weber, *Phys. Rev. B* **31**, 5262 (1985).
- ⁴⁵G. J. Martyna, M. E. Tuckerman, D. J. Tobias, and M. L. Klein, *Mol. Phys.* **87**, 1117 (1996).
- ⁴⁶W. G. Hoover, *Phys. Rev. A* **31**, 1695 (1985).
- ⁴⁷S. Nosé, *J. Chem. Phys.* **81**, 511 (1984).
- ⁴⁸J. Nocedal, *Mathematics of Computation* **35**, 773 (1980).
- ⁴⁹D. C. Liu and J. Nocedal, *Mathematical Programming* **45**, 503 (1989).
- ⁵⁰J. M. Soler, E. Artacho, J. D. Gale, A. García, J. Junquera, P. Ordejón, and D. Sánchez-Portal, *Journal of Physics: Condensed Matter* **14**, 2745 (2002).
- ⁵¹N. Troullier and J. L. Martins, *Phys. Rev. B* **43**, 1993 (1991).
- ⁵²L. Kleinman and D. M. Bylander, *Phys. Rev. Lett.* **48**, 1425 (1982).
- ⁵³J. P. Perdew, K. Burke, and M. Ernzerhof, *Phys. Rev. Lett.* **77**, 3865 (1996).
- ⁵⁴J. Harris, *Phys. Rev. B* **31**, 1770 (1985).
- ⁵⁵J. P. Perdew and A. Zunger, *Phys. Rev. B* **23**, 5048 (1981).
- ⁵⁶K. Laaziri, S. Kycia, S. Roorda, M. Chicoine, J. L. Robertson, J. Wang, and S. C. Moss, *Phys. Rev. B* **60**, 13520 (1999).
- ⁵⁷D. Beeman, R. Tsu, and M. F. Thorpe, *Phys. Rev. B* **32**, 874 (1985).
- ⁵⁸P. J. Steinhardt, D. R. Nelson, and M. Ronchetti, *Phys. Rev. B* **28**, 784 (1983).
- ⁵⁹W. A. Kamitakahara, H. R. Shanks, J. F. McClelland, U. Buchenau, F. Gompf, and L. Pintschovius, *Phys. Rev. Lett.* **52**, 644 (1984).
- ⁶⁰Since the energy associated with vibrational excitations in solids, involving a fraction of an electron-volt, is significantly smaller than their electronic counterpart (with a few to several electron-volts), a small perturbation in the local atomic environment of atoms can be readily manifested in the vibrational spectrum of a solid. At high temperature, such effects can be considerably weakened or washed out due to thermal broadening.
- ⁶¹S. V. Khare, S. M. Nakhmanson, P. M. Voyles, P. Keblinski, and J. R. Abelson, *Applied Physics Letters* **85**, 745 (2004).
- ⁶²J. Gibson, M. Treacy, and P. Voyles, *Ultramicroscopy* **83**, 169 (2000).
- ⁶³P. Biswas, R. Atta-Fynn, S. Chakraborty, and D. A. Drabold, *Journal of Physics: Condensed Matter* **19**, 455202 (2007).
- ⁶⁴P. Biswas, D. N. Tafen, R. Atta-Fynn, and D. Drabold, *Journal of Physics: Condensed Matter* **16**, S5173 (2004).